Supporting Material

NMR-detected Brownian dynamics of αB-crystallin over a wide range of concentrations

Matthias Roos, Susanne Link, Jochen Balbach, Alexey Krushelnitsky,* Kay Saalwächter*

Institut für Physik, Martin-Luther-Universität Halle-Wittenberg,
Betty-Heimann-Str. 7, 06120 Halle (Saale), Germany.

Sample preparation.

Protein expression and purification of human αB-crystallin.

After cloning the human αB cDNA into a modified, His-tag free pET16b vector and expression in *Escherichia coli* BL21(DE3), protein expression and purification were performed in a manner similar to ref. (1). Briefly, αB-crystallin was expressed overnight at 22°C in the auto-induction media ZYM 5052, lysed by Microfluidizer in 20mM TrisHCL (pH 8.5) and 1mM EDTA buffer, the DNA digested by DNase1 and precipitated by protamine sulfate salt. After purification on a TMAE anion-exchange column with a stepwise NaCl gradient, αB fractions were pooled, concentrated and loaded on a S200 gel filtration column with a running buffer containing 20mM TrisHCL (pH 7.5), 50mM NaCl and 1mM EDTA. The purity of the protein was confirmed by SDS-page and mass spectrometry.

NMR sample preparation.

After extensive dialysis against 50mM ammonium hydrogen carbonate buffer (pH 8), the protein was lyophilized, then dissolved in the smaller amount of the same buffer in D_2O and lyophilized again. Note that multiple lyophilization does not affect αB-crystallin properties, as confirmed by NMR spectroscopic and diffusion experiments. The lyophilized αB-crystallin powder was

dissolved in 50mM Na-phosphate buffer, 50mM NaCl and 0.002% NaN_3 D_2O buffer at pH 7.6 (pD=7.2) and used in the NMR and viscosity measurements. The αB-crystallin concentration was determined by spectral photometry at 280 nm with MW=20027.7 Da and ε=13980 M cm^{-1}.

NMR experiments.

Translational diffusion

Translational self-diffusion coefficients were measured using the stimulated echo technique with bipolar pulsed field gradients (2). Fig. S1 shows proton spectra of αB-crystallin in D_2O buffer after a 90º-pulse (top). The strong signal at ~5 ppm corresponds to residual solvent protons that cannot be fully removed during the sample preparation. The NMR spectrum seen in the PFG experiments is shown at the bottom, in which the water signal is filtered out on the basis of its fast diffusion. A large fraction of the protein signal is also filtered out due to the short T_2 of the residues forming the rigid core, while the remaining signal belongs to the protons of mobile unstructured termini of αB-crystallin polypeptide chains that have long T_2. It is noted that without these unstructured termini the PFG measurement of translational diffusion would be impossible: αB-crystallin is a large protein, so its overall rotational tumbling is slow. If all parts of the protein were rigid, then the complete protein signal would be T_2-filtered (suppressed) during the field gradient pulse, which has a typical duration of 1 - 1.5 ms.

Analyses of the diffusion decay are based upon the right-hand side peak belonging to methyl protons, as marked by an arrow in Fig. S1. Fig. S2 compares the PFG NMR diffusion decay of the integral signal to that of the methyl protons peak. It is clearly seen that the two decays differ, with the difference becoming more pronounced at higher concentrations. Such a difference can be explained by the effect of spin diffusion between protein protons combined with hydrogen exchange of labile protein protons with the residual solvent protons. Thus, the apparent diffusion decay for the integral protein signal is distorted by the magnetic/chemical exchange processes (3,4). This effect is negligible in small and medium-sized proteins because spin diffusion is rather slow due to the much faster overall rotational tumbling, which averages out inter-proton dipole-dipole interactions. The methyl protons are less prone to such distortions since they undergo fast rotation around the C_3 axis, and thus have weak magnetic coupling to other protein protons.

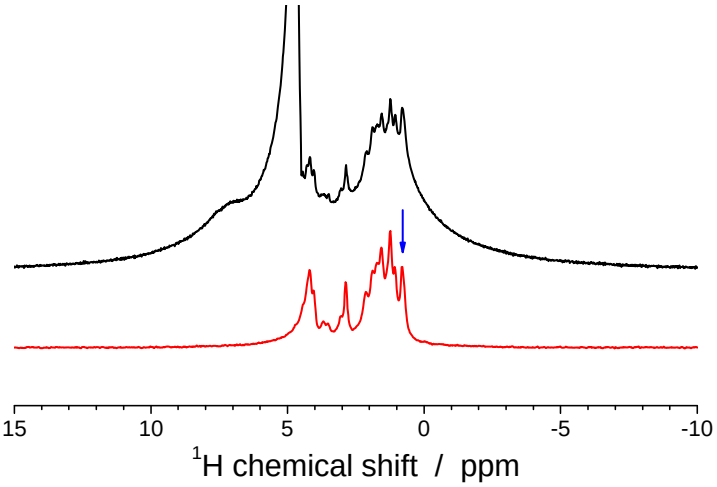

Figure S1. Proton NMR spectrum of αB-crystallin at 400 MHz resonance frequency after a 90º pulse (top), and after T_2/diffusion filtering during the pulse-gradient experiment (bottom). The blue arrow indicates the peak which was used for evaluating the diffusion decays.

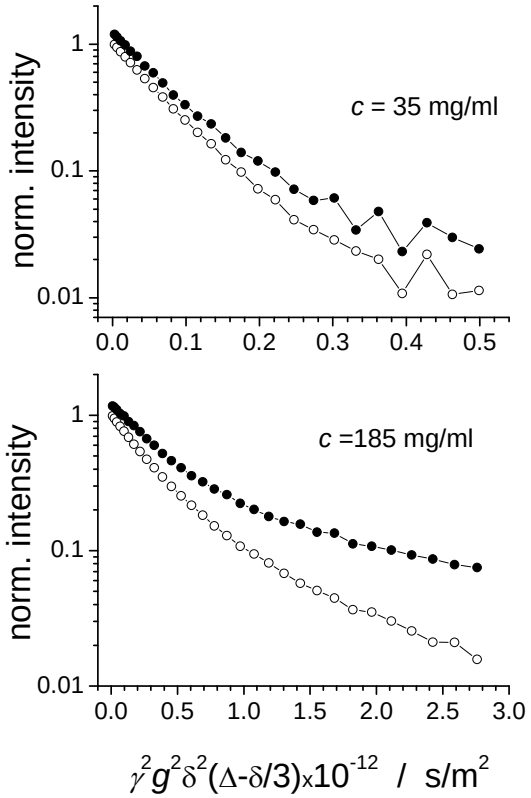

Figure S2. Diffusion decays for αB-crystallin solution at two concentrations (T = 20 ºC) plotted for the integral signal (open circles) and the methyl peak marked by an arrow in Fig. S1 (solid circles).

Fig. S3 compares the diffusion decays measured at two different diffusion times (Δ). The SDC should not depend on Δ, however, if the characteristic time of the magnetic/chemical exchange processes is comparable to Δ, then the apparent diffusion decay will become faster as Δ increases. It is seen that the diffusion decay at Δ = 300 ms is indeed somewhat faster, yet the difference is negligibly small. In our PFG experiments Δ was always between 25 and 40 ms, thus the effect of the magnetic/chemical exchange can be safely neglected.

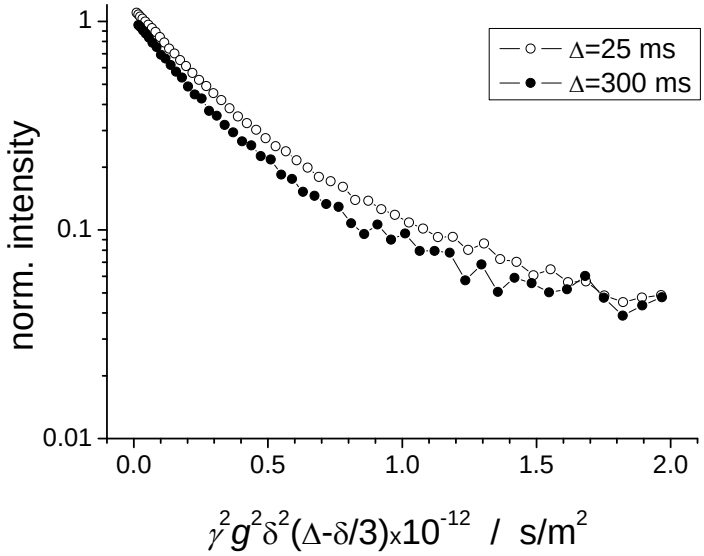

Figure S3. Diffusion decays measured at two different diffusion times (indicated in the plot) plotted for the methyl protons peak (c = 185 mg/ml, T = 28 ºC).

Spin relaxation

On-resonance $T_{1\rho}$'s at 20 and 40 kHz spin-lock frequencies were measured with the standard pulse sequence, Fig. S4. Off-resonance $T_{1\rho}$'s at 60 kHz were measured with the sequence shown in Fig. S5a. The latter sequence starts with two 90º-pulses, of which the first pulse is of fixed phase, while the second one is phase-alternated to ensure spin temperature inversion. In doing so, the relaxation signal decays exactly to zero, thus there is no need to measure the long relaxation delay plateau. In addition, the off-resonance spin-lock pulse is flanked by two orienting off-resonance 180º-pulses: the first orienting pulse aligns the magnetization vector along the B_{1e} field and the second one brings the magnetization back to B_0 direction. By this, the orienting pulse vector forms the angle $\theta/2$ with the B_0 (and B_{1e} as well) vector, see Fig. S5b.

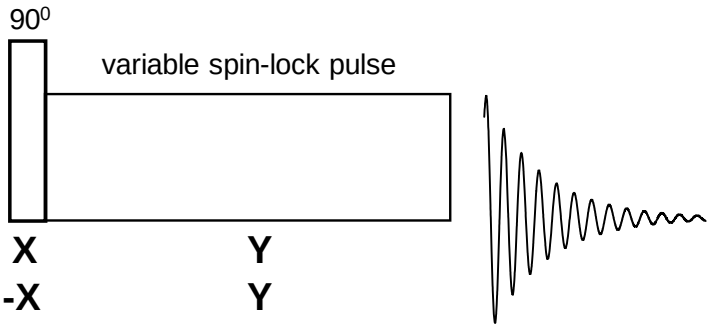

Figure S4. Pulse sequence for measuring $T_{1\rho}$ decays with on-resonance spin-lock field.

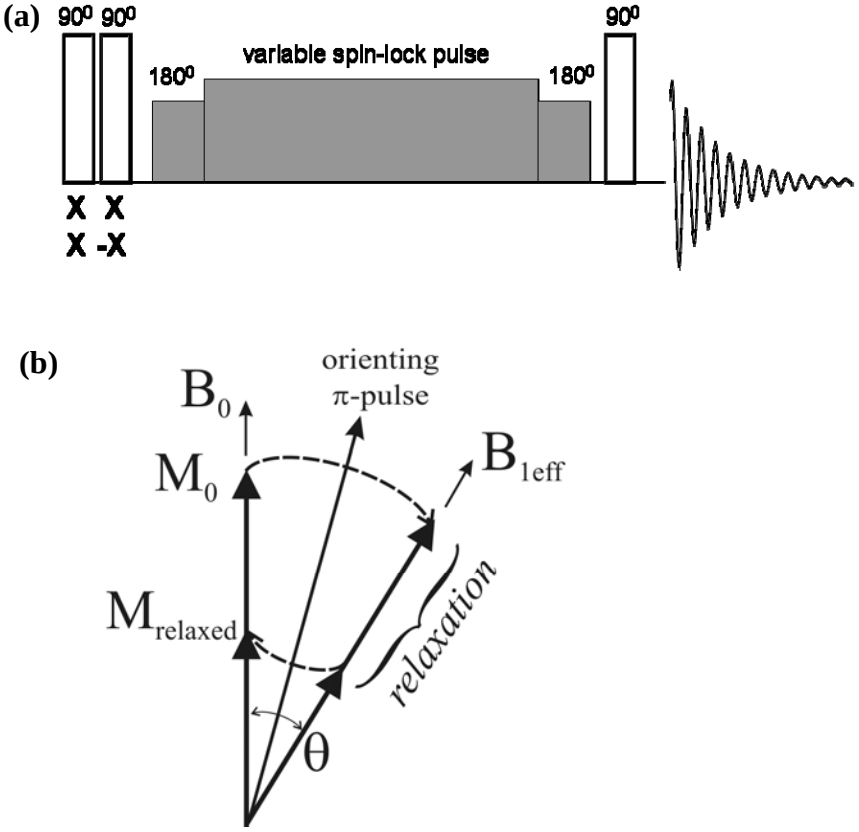

Figure S5. (a) Pulse sequence for measuring off-resonance $T_{1\rho}$. Shaded pulses are applied with the resonance offset. (b) Vector scheme demonstrating magnetization perturbations during the off-resonance pulses.

Before each $T_{1\rho}$ measurement the spin-lock frequencies and the angle θ (for the off-resonance experiments) were carefully calibrated using a nutation experiment. For all the off-resonance measurements the angle θ was equal to 42º. The spin-lock field duration in the $T_{1\rho}$ experiments

was varied from few μs to 200 ms. For plotting the relaxation decays, the whole spectral window (see Fig. S1, top) was used for integration of the proton signal. To avoid sample heating by long spin-lock pulses, the recycling delay was 20 s. The chemical shift of the residual water protons peak did not depend on the duration of the spin-lock pulse which confirms that the sample heating effect was negligible.

Spin-spin (T_2) relaxation decays were measured by a combination of three different experiments: Free induction decay (FID; time range from 12 (dead time) to 40 μs), Hahn echo (from 30 μs to ~3 ms) and a Carr-Purcell-Meiboom-Gill sequence (from 0.5 ms to ~0.4 s). This was done in order to cover a wide range of the relaxation times, as the protein T_2 is very short, usually tens to hundreds of μs, whereas the solvent T_2 was of the order of hundreds of ms. Since T_2 relaxation decays were measured at the resonance frequency 20 MHz and imperfect B_0 field homogeneity, no spectral resolution could be achieved at these conditions and thus, the decays were recorded directly in the time domain.

The analysis of the $T_{1\rho}$ and T_2 relaxation decays was performed according to the procedure described in ref. (5). As mentioned above, protein solutions contain a certain amount of residual solvent protons which exhibit much longer $T_2/T_{1\rho}$'s, thus requiring to subtract the solvent signal for analyzing the unbiased protein signal (cf. Fig. S6). For plots and analyses, the relaxation decays of the total (integral) proton signal was detected without any spectroscopic separation in both the $T_{1\rho}$ and T_2 experiments. The water signal subtraction procedures (Fig. S6) for the T_2 and $T_{1\rho}$ decays were fully identical.

After subtraction of the solvent signal we obtained the protein protons' relaxation decay, which is of multi-exponential shape (Fig. S6). This decay reflects a wide distribution of the relaxation times which is a consequence of the dynamic heterogeneity of α-crystallin. For such a decay we determined the mean relaxation rate/time, which equals the slope of the initial part of the decay. In practice, we fitted the decays with a sum of two exponential components, which provides a minimal fitting model. We then determined the mean relaxation rate as

$$\left\langle \frac{1}{T_2} \right\rangle = \frac{1}{P_a + P_b}\left(\frac{P_a}{T_{2a}} + \frac{P_b}{T_{2b}} \right),$$

where $P_{a,b}$ and $T_{2a,b}$ are the intensities and relaxation times of the two components, respectively (taken separately, these parameters have no physical meaning).

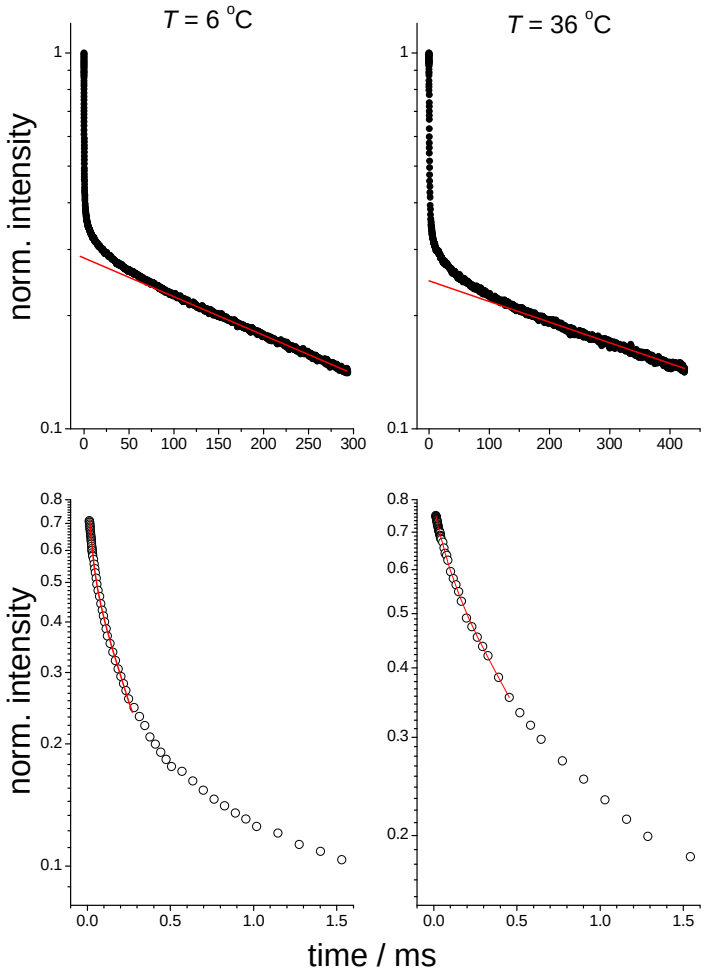

Figure S6. T_2-relaxation decays measured for αB-crystallin solutions at c =80 mg/ml and two temperatures (indicated in the figure). $T_{1\rho}$-decays have very similar shapes. *Top:* raw relaxation decays consisting of the fast (protein) and slow (solvent) relaxing components. Red lines indicate the solvent component that was defined from the exponential fit of the slow tail of the relaxation decay. *Bottom:* the protein relaxation signal after the subtraction the solvent component from the overall decay. Red curves correspond to the biexponential fit of the initial part of the decay, which was used for the determination of the mean relaxation time (initial slope of the decay) as described in the text. Possible cross-relaxation (spin diffusion) between protein protons may change the form of the relaxation decay, but the mean relaxation rate (initial slope) does not depend on this.

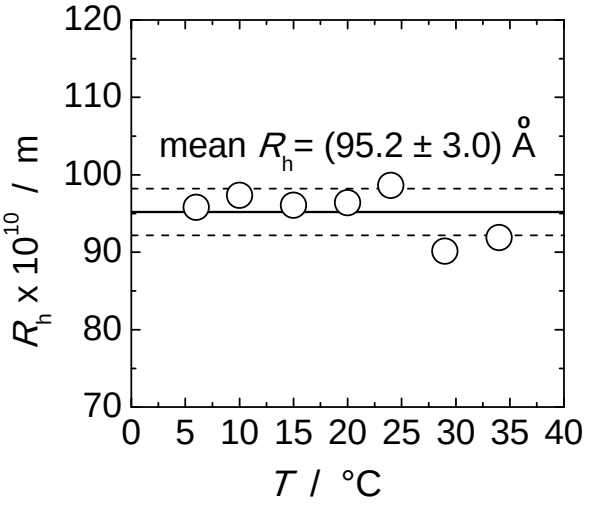

Figure S7. Hydrodynamic radii of αB-crystallin as determined via the Stokes-Einstein relationship with independent measurements of the viscosity and translational self-diffusion at a concentration of 35 mg/ml. The solid and dashed lines indicate the mean value of all points and their standard deviation, respectively.

Fitting the temperature dependences of the relaxation times: (i) distribution of correlation times. Taking into account the intrinsic size distribution of α-crystallin, as also reflected in the PFG NMR diffusion decays, it is worthy to estimate the impact of a distribution of τ_{rot} on the fitting result of the T_2 and $T_{1\rho}$ data. To simulate a τ_{rot} distribution, the fast component was represented by a spread of 3 modes on a logarithmic scale, namely 2/3 $\tau_{rot,}$ τ_{rot}, and 3/2 $\tau_{rot,}$ with relative amplitudes of ¼, ½ and ¼ for the faster, main and slower component, respectively. The total spectral density function addressing the fast component thus reads

$$J_{fast}(\omega;\tau_{rot}) = \tfrac{1}{4} J(\omega;\tfrac{2}{3}\tau_{rot}) + \tfrac{1}{2} J(\omega;\tau_{rot}) + \tfrac{1}{4} J(\omega;\tfrac{3}{2}\tau_{rot})$$

and reflects a relative standard deviation of τ_{rot} of approx. 35%. As a consequence, this broadens the minimum of the $T_{1\rho}$ curves, yet such a spread of τ_{rot} values was not found to have an appreciable effect on the quality of the fitting result (cf. Fig. S8) and the fitting values obtained (cf. Table S1). In fact, the relative increase of the mean τ_{rot} was found to be in good accordance with the previous results when modeling the experimental data using a single value of τ_{rot} only. Thus, introducing a spread of τ_{rot} is not reasonable since it does not change significantly the fitting

results, at the same time making fitting less certain by increasing the number of fitting parameters.

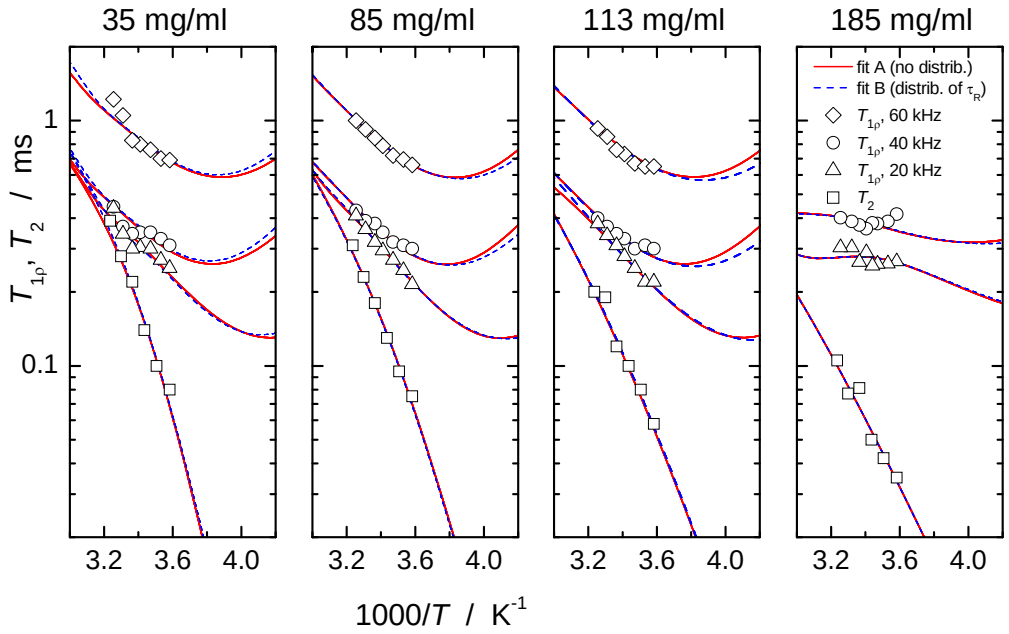

Figure S8. T_2 and $T_{1\rho}$ relaxation times (see legend) with their best fit results (lines) by use of a distribution of the fast component τ_{rot} (dashed lines) in comparison to the fitting result using a single value of τ_{rot} (solid lines).

Table S1. Summary of the fitting result by reflecting the fast component (τ_{rot}) by one mode only (model A) in comparison to the outcome assuming a logarithmic spread of τ_{rot} with a standard deviation of about 35% (model B, see explanation in the text). $<\tau_{rot}>$ for the model (B) was calculated as $\langle\tau_{rot}\rangle^{-1} = \frac{1}{4}\left(\frac{2}{3}\tau_{rot}\right)^{-1} + \frac{1}{2}(\tau_{rot})^{-1} + \frac{1}{4}\left(\frac{3}{2}\tau_{rot}\right)^{-1}$. $\langle R_{rot}\rangle$ was calculated according to Eq. 11 of the main paper.

Model	τ	35 mg/ml	85mg/ml	113 mg/ml	185mg/ml
(A)	τ_{rot} / μs	0.90±0.02	0.96±0.02	1.03±0.02	1.04±0.02
	$\langle R_{rot}\rangle^{-1}$ / μs	0.91±0.05	0.98±0.05	1.05±0.05	1.31±0.05
	$\langle R_{rot}\rangle(c_1)/\langle R_{rot}\rangle(c_i)$	**1.00**	**1.08±0.02**	**1.15±0.02**	**1.44±0.04**
(B)	$<\tau_{rot}>$ / μs	0.85±0.02	0.89±0.02	0.97±0.02	0.96±0.02
	$\langle R_{rot}\rangle^{-1}$ / μs	0.86±0.05	0.91±0.05	0.99±0.05	1.17±0.05
	$\langle R_{rot}\rangle(c_1)/\langle R_{rot}\rangle(c_i)$	**1.00**	**1.05±0.02**	**1.16±0.02**	**1.36±0.04**

Fitting the temperature dependences of the relaxation times: (ii) K_{HH}^{av} temperature dependence. In the analysis we assume K_{HH}^{av} to be temperature independent although the amplitude of internal motions in proteins may depend on temperature (6,7). To check the influence of the possible K_{HH}^{av} temperature dependence on the fitting results, we performed the fitting assuming a simple linear dependence of K_{HH}^{av} on temperature. Direct measurements of K_{HH}^{av} in solid hydrated proteins at different temperatures (8,9) show that within temperature range of our experiments (from ~5 ºC to ~35 ºC) K_{HH}^{av} varies no more than 10-20%. Note that this temperature variation is caused not only by the change of motional amplitude, but mainly by the temperature dependence of the correlation times of internal motions which affects the motional averaging of the proton second moment. Therefore, we fitted the data assuming the 15% difference of K_{HH}^{av} between 5 and 35 ºC. The fitting curves in this case look the same as in Fig. S8 or Fig. 3 of the main paper. The comparison of the fitting results (Table S2) with those assuming temperature independent K_{HH}^{av} (Table 1 of the main paper) demonstrates that the K_{HH}^{av} temperature dependence affects only the absolute value of K_{HH}^{av} and the activation energy E_{rot}. All other parameters remain the same.

Table S2. Dynamic parameter obtained from the fitting assuming K_{HH}^{av} to be temperature dependent. K_{HH}^{av} at 20 ºC is $(3.7\pm0.1)\cdot10^{9}$ s^{-2}.

c / mg/ml	τ_{rot} / μs at 20 ºC	$S_{\mathrm{rot}}^2\ \tau_{\mathrm{S}}$ / μs at 20 ºC	E_{rot} / kJ/mol	E_{s} / kJ/mol
35	0.92±0.02	0.65±0.02	12±1	63±2
85	0.97±0.02	0.84±0.02	13±1	49±2
113	1.04±0.03	1.38±0.03	12±1	38±2
185	1.07±0.03	3.73±0.07	2±1	27±1

Here, we would like to also demonstrate that the assumption of the possibly steeper temperature dependence of K_{HH}^{av} cannot describe the data well without taking into account the slow component of the $C_t(t)$, i.e. assuming S_{rot}^2 =0. We performed the data fitting assuming S_{rot}^2 =0 and the slope of the K_{HH}^{av} temperature dependence as an additional free fitting parameter. As a result, we obtained a bad fitting quality (see Fig. S9) and a rather unreasonable temperature variation of K_{HH}^{av} of about 40% between 5 and 35 ºC. Thus, the assumption of the K_{HH}^{av} temperature dependence has no significant influence on our results.

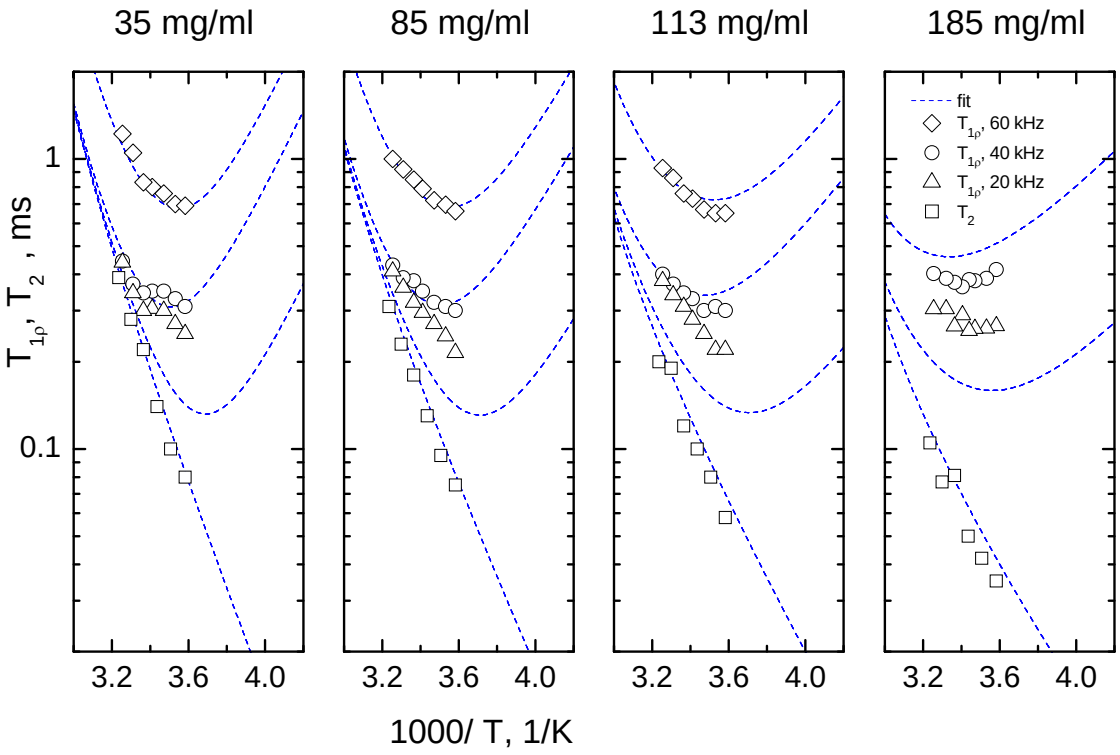

Figure S9. Fitting results assuming K_{HH}^{av} to be temperature-dependent, and S_{rot}^2 =0.

Fitting the temperature dependences of the relaxation times: (iii) fixed ratio between the correlation times. Fig. S10 shows fits for which we tried a ratio between the correlation times fixed to

τ_{rot}(35 mg/ml): τ_{rot}(85 mg/ml): τ_{rot}(113 mg/ml): τ_{rot}(185 mg/ml) = 1.00 : 1.67 : 2.20 : 6.00,

which corresponds to the relative increase in viscosity (or the translational diffusion slow-down). Obviously, this results in a strong mismatch between the fitting curves and the experimental data.

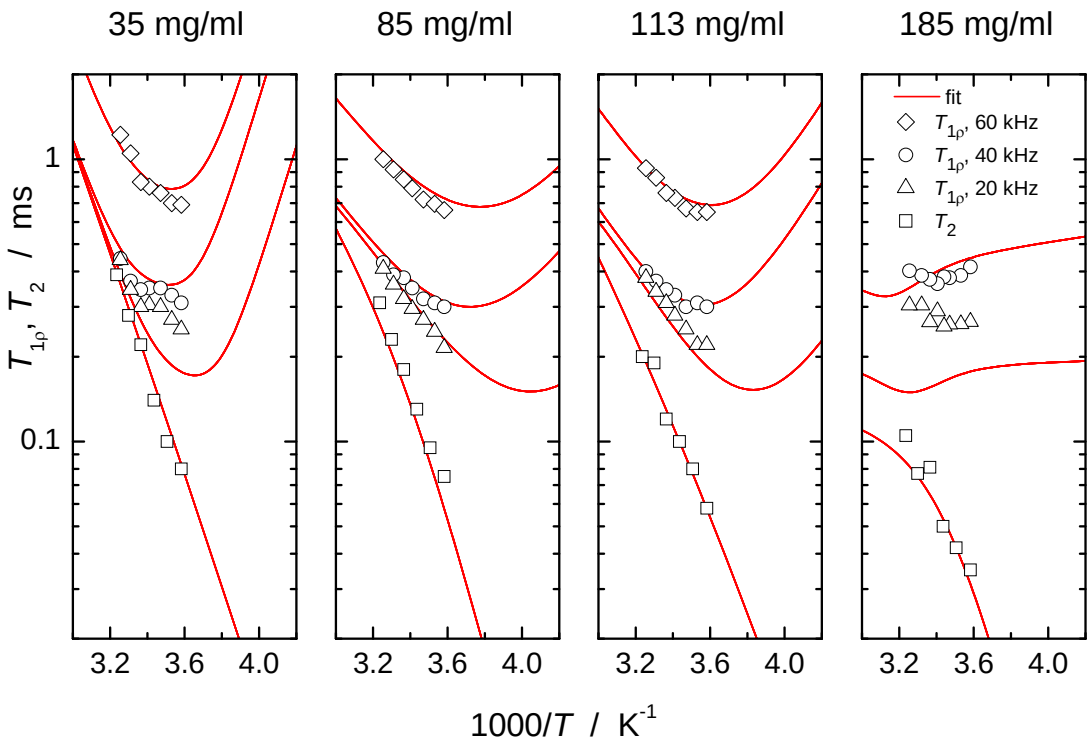

Figure S10. T_2 and $T_{1\rho}$ relaxation times with their best fit results (red lines) by use of a fixed ratio of the rotational correlation time τ_{rot} following the retardation of translational diffusion.

Rotational correlation time vs. molecular mass: statistics of literature data.

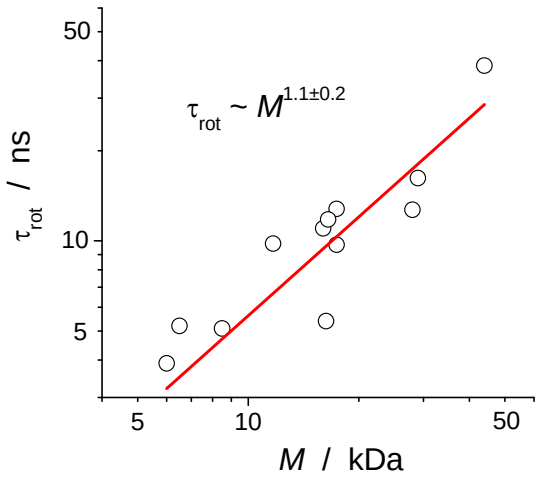

Figure S11. Rotational correlation time as a function of the protein M for 12 different proteins. All correlation times were recalculated for the temperature 20 ºC, the details being presented in Table S3. It is clearly seen that the slope can be defined only with a large uncertainty.

Table S3. Collection of rotational correlation times for 12 different proteins. In all cases the correlation time was defined from the ^{15}N T_1/T_2 ratio. Since the temperatures of the measurements were different, all the correlation times were recalculated to 20 ºC using the Arrhenius dependence and an activation energy of 20 kJ/mol. Fig. S8 was plotted using the numbers in bold (2nd and 5th columns).

Protein	MM, kDa	T / ºC	τ_{rot} / ns	τ_{rot} (20ºC)	Reference
Interleukin 1β	**17.4**	36	8.3	**12.8**	Clore GM, Driscoll PC, Wingfield PT, Gronenborn AM (1990), *Biochemistry* 29: 7387–7401.
calbindin D9k	**8.5**	27	4.2	**5.1**	Kordel J, Skelton NJ, Akke M, Palmer AG, Chazin WJ (1992), *Biochemistry* 31: 4856–4866.
Bacillus-subtilis glucose perme-ase-IIA domain	**17.4**	35	6.5	**9.7**	Stone MJ et al. (1992), *Biochemistry* 31: 4394–4406.
Thioredoxin	**11.7**	35	6.55	**9.8**	Stone MJ, Chandrasekhar K, Holmgren A, Wright PE, Dyson HJ (1993), *Biochemistry* 32: 426–435.
Interleukin-8	**16**	27	9.1	**11.0**	Grasberger BL, Gronenborn AM, Clore GM (1993), *J Mol Biol* 230: 364–372.
Igg binding domain	**6**	26	3.3	**3.9**	Barchi JJ, Jr., Grasberger B, Gronenborn AM, Clore GM (1994), *Prot Sci* 3: 15–21.
Ribonuclease HI	**16.5**	27	9.7	**11.8**	Mandel AM, Akke M, Palmer AG (1995), *J. Mol Biol* 246: 144–163.
Savinase	**28**	30	9.7	**12.7**	Remerowski ML, Pepermans HAM, Hilbers CW, Van De Ven FJM (1996), *Eur J Biochem* 235: 629–640.

SH3 domain	**6.5**	7	7.6	**5.2**	Chevelkov V, Zhuravleva AV, Xue Y, Reif B, Skrynnikov NR (2007), *J Am Chem Soc* 129: 12594–12595.
Flavodoxin	**16.3**	27	4.5	**5.4**	Hrovat A, Blümel M, Löhr F, Mayhew SG, Rüterjans H (1997), *J Biomol NMR* 10: 53–62.
Ectodomain of SIV gp41	**44**	45	20	**38.5**	Caffrey M, Kaufman J, Stahl SJ, Wingfield PT, Gronenborn AM, Clore GM (1998), *J Magn Reson* 135: 368 –372.
TEM-1 β-lactamase	**29**	30	12.4	**16.2**	Savard PY, Gagne SM (2006), *Biochemistry 45*: 11414-11424.

References.

(1) Mainz, A., S. Jehle, B.J. van Rossum, H. Oschkinat, and B. Reif (2009). Large protein complexes with extreme rotational correlation times investigated in solution by magic-angle-spinning NMR spectroscopy. *J Am Chem Soc* 131: 15968-15969. (Supporting Information)

(2) Cotts R.M., M.J.R. Hoch, T. Sun, and J.R. Markert (1989). Pulsed Field Gradient Stimulated Echo Methods for Improved NMR Diffusion Measurements in Heterogeneous Systems. *J Magn Reson* 83: 252-266.

(3) Chen A., C.S. Johnson Jr., M. Lin, and M.J. Shapiro (1998). Chemical Exchange in Diffusion NMR Experiments. *J Am Chem Soc* 120: 9094-9095.

(4) Andrec M, and J.H. Prestegard (1997). Quantitation of chemical exchange rates using pulsed-field-gradient diffusion measurements. *J Biomol NMR* 9: 136-150.

(5) Krushelnitsky, A.G., and V.D. Fedotov (1993). Overall and internal protein dynamics in solution studied by the nonselective proton relaxation. *J Biomol Struct Dyn* 11:121-141.

(6) Chang, S.-L., and N. Tjandra (2005). Temperature dependence of protein backbone motion from carbonyl ^{13}C and amide ^{15}N NMR relaxation. *J Magn Reson* 174: 43-53.

(7) Johnson, E, A.G. Palmer, and M. Rance (2007). Temperature dependence of the NMR generalized order parameter. *Prot Str Func Bioinf* 66: 796-803.

(8) Blears, D.J and S.S.Danyluk (1968). Proton wide-line nuclear magnetic resonance spectra of hydrated proteins. *Biochim Biophys Acta* 154: 17-27.

(9) Krushelnitsky, A.G., V.D. Fedotov, J. Spevacek, and J. Straka (1996). Dynamic structure of proteins in solid state. ^{1}H and ^{13}C NMR relaxation study. *J Biomol Struct Dyn* 14: 211-224.